Properties of a $Ni_{19.5}Pd_{30}Ti_{50.5}$ high-temperature shape memory alloy in tension and compression

Ronald Noebe[#], Santo Padula, II[#], Glen Bigelow[#], Orlando Rios[+], Anita Garg[#], and Brad Lerch[#]
[#]NASA Glenn Research Center, Materials & Structures Division, Cleveland, OH 44135
[+]University of Florida, Dept. of Materials Science & Engineering, Gainesville, FL 32611

ABSTRACT

Potential applications involving high-temperature shape memory alloys have been growing in recent years. Even in those cases where promising new alloys have been identified, the knowledge base for such materials contains gaps crucial to their maturation and implementation in actuator and other applications. We begin to address this issue by characterizing the mechanical behavior of a $Ni_{19.5}Pd_{30}Ti_{50.5}$ high-temperature shape memory alloy in both uniaxial tension and compression at various temperatures. Differences in the isothermal uniaxial deformation behavior were most notable at test temperatures below the martensite finish temperature. The elastic modulus of the material was very dependent on strain level; therefore, dynamic Young's Modulus was determined as a function of temperature by an impulse excitation technique. More importantly, the performance of a thermally activated actuator material is dependent on the work output of the alloy. Consequently, the strain-temperature response of the $Ni_{19.5}Pd_{30}Ti_{50.5}$ alloy under various loads was determined in both tension and compression and the specific work output calculated and compared in both loading conditions. It was found that the transformation strain and thus, the specific work output were similar regardless of the loading condition. Also, in both tension and compression, the strain-temperature loops determined under constant load conditions did not close due to the fact that the transformation strain during cooling was always larger than the transformation strain during heating. This was apparently the result of permanent plastic deformation of the martensite phase with each cycle. Consequently, before this alloy can be used under cyclic actuation conditions, modification of the microstructure or composition would be required to increase the resistance of the alloy to plastic deformation by slip.

Keywords: High-temperature shape memory alloy, NiTiPd, tensile properties, compression, specific work output, shape memory behavior, dynamic modulus, transformation strain, transformation temperatures.

1.0 INTRODUCTION

Ever since the shape memory phenomenon was observed in NiTi alloys, the number of potential applications for this functional material has continued to grow. General applications include use in couplings, electrical interconnects, high-force actuators for automotive, aeronautic, and robotic applications, temperature sensitive flow control devices, and numerous other applications that can benefit from the unique properties of shape memory or superelastic behavior. Nevertheless, many desired applications for shape memory alloys never reach fruition because of the inherent temperature limitations of binary Ni-Ti alloys, which have a maximum martensite start temperature (M_s) of about 60 °C [1]. In contrast to the relatively low transformation temperatures in Ni-Ti alloys, binary alloys based on precious metal-Ti compositions such as PdTi exhibit martensitic transformations with M_s temperatures exceeding 500 °C [2]. PdTi and NiTi also form a continuous solid solution with a high-temperature B2 phase that transforms to a B19 (orthorhombic) or B19' (monoclinic) low-temperature martensite phase with transformation temperatures between those of the binary alloys [3]. It has also been confirmed that the martensitic transformations over the entire range of ternary Ni-Pd-Ti compositions are thermoelastic in nature and that the alloys exhibit aspects of shape memory behavior similar to binary NiTi alloys [4,5]. Since then, work on ternary NiTiPd alloys has intensified because of their potential for use in high temperature applications.

Shimizu et al. [6] examined the effect of stoichiometry ((Ni+Pd):Ti ≠ 50:50) on the transformation temperatures of a series of $Ti_{50-x}Pd_{30}Ni_{20+x}$ alloys (where x = -0.6 to 1.5 at.%). An extremely steep drop in transformation temperature was observed for Ti-deficient alloys but only a moderate change in transformation temperature was observed on the Ti-rich side of stoichiometry where fine Ti_2Ni type precipitates were reported to form after aging at 500 °C. This effect of

stoichiometry on the transformation temperatures for NiPdTi alloys is consistent with binary NiTi alloys where there is a very steep drop in transformation temperatures for Ti-deficient compositions and nearly constant transformation temperatures with Ti content for stoichiometric and Ti-rich compositions [1].

The shape memory behavior of NiTi-30Pd (at.%) alloys has been studied in some detail. Tensile samples loaded to 2-4% total strain in the martensitic condition were capable of recovering 100% of that strain through various mechanisms and almost 90% of the strain could be recovered in samples loaded to 6% total strain [5,6,7]. Similar shape memory behavior has been observed for samples deformed in compression [8] and torsion [9]. However, for alloys containing 40 at.% or more Pd including the TiPd binary alloy, only about 0.5% strain could be recovered in alloys loaded in tension to various strain levels [5,10]. This limited amount of strain recovery has been attributed to a low critical stress for slip (which is an irreversible process), such that the majority of the deformation is accommodated by slip rather than the more typical twin boundary motion or martensite reorientation (also referred to as detwinning) [10]. A number of studies have since been performed that have focused on improving the shape memory behavior of NiTiPd alloys through various mechanisms aimed at enhancing the alloys resistance to slip and thus promoting greater deformation by twin motion in hopes of enhancing the stress-free shape memory behavior of these alloys. Such studies have involved the use of solid solution strengthening [8,11], precipitate strengthening [6], and various thermomechanical processing routines [12,13], with little success in the former and moderate success with the other approaches.

To the authors' knowledge, all the work published to date on the functional behavior of NiTiPd alloys has involved recovery of strains under stress free conditions. However, the most likely applications for high temperature shape memory alloys involve their use as actuator materials, where the material recovers against an applied or biasing stress, thus performing work on a system. It should be noted that work can be extracted from NiTi shape-memory alloys at energy densities exceeding 10 J/cm^3 [14], making binary NiTi alloys very intriguing for use as solid state actuators. However, recovery of NiTiPd alloys under stress has not been previously investigated and no direct studies comparing the general tensile and compression behavior of NiTiPd alloys have been reported. Consequently, a detailed study of the behavior of a $Ni_{19.5}Pd_{30}Ti_{50.5}$ alloy under tensile and compression loading including the strain-temperature response of the alloy under various constant stresses was performed to determine the work characteristics of this potential high temperature shape memory alloy.

2.0 MATERIALS AND PROCEDURES

2.1 Material Processing and Characterization

An alloy of target composition $Ni_{19.5}Pd_{30}Ti_{50.5}$ (all compositions are noted in atomic percent) was chosen for analysis, because the slight Ti-rich composition would help ensure a high transformation temperature [6]. Ingots were prepared by vacuum induction melting of high purity elemental constituents (99.95 Ti, 99.995 Pd, 99.98 Ni) in a graphite crucible. The induction melter was equipped with tilt-pour capability and the melts were cast into a cylindrical copper mold 25.4 mm in diameter by 102 mm in length, with an appropriate hot top to accommodate shrinkage during solidification. Prior to extrusion, the ingots were homogenized in a vacuum furnace at 1050C °C for 72 h. The ingots were subsequently placed into mild steel extrusion cans, which were evacuated and sealed. The extrusion process was performed at 900 °C and a 7:1 area reduction ratio. The chemical composition was determined for all materials after extrusion by inductively coupled plasma spectroscopy and by conventional N/O and C/S determination.

Rough blanks for cylindrical shaped compression samples were cut from the extruded bars by electrical discharge machining (EDM) and centerless ground to final diameter. The finished specimens were 5 mm in diameter by 10 mm in length. Cylindrical dog-bone-shaped tensile samples were cut from appropriate lengths of the extrusion rod using a computer controlled lathe. The total length of each sample was 50.8 mm with threaded button ends. The gage section of each of the tensile samples was 17.4 mm long by 3.81 mm diameter. Both tension and compression samples were tested in the direction parallel to the original extrusion axis. To complete the sample preparation phase, all samples were given a stress relief heat treatment at 400 °C for 1 hour followed by a furnace cool prior to testing. The function of this heat treatment was to relieve any residual stresses due to the extrusion and machining processes.

The microstructure of the extruded $Ni_{19.5}Pd_{30}Ti_{50.5}$ alloy after the stress relief treatment was examined by conventional scanning electron microscopy (SEM) and transmission electron microscopy techniques (TEM). Samples for SEM were

mounted and metallographically polished prior to examination in the SEM. A JEOL 840 and Hitachi 6100 equipped with energy-dispersive spectroscopy (EDS) capability were used to determine the basic microstructure of the alloy and to obtain an indication of the volume fraction and composition of any additional phases present. TEM samples were prepared by cutting 3mm diameter by 0.5 mm thick disks by EDM. These disks were subsequently ground to a thickness of approximately 0.1 mm, dimpled, and then ion milled to final electron transparency. TEM analysis including electron diffraction and EDS analysis was performed on the second phase particles in order to conclusively identify all phases present using a Phillips 400T or CM200 microscope. X-ray analysis was used to determine the structure and lattice parameters of the martensite phase.

Transformation temperatures and the temperature dependent electrical properties of the $Ni_{19.5}Pd_{30}Ti_{50.5}$ alloy in the stress free condition and in-situ during mechanical testing were determined by high resolution resistivity measurements. The samples were instrumented with a four point probe and a K-type thermocouple each of which were spot welded directly to the sample surface. A four point probe configuration was chosen in order to eliminate the effects of contact resistance. Pt or Ni wires were spot welded to the sample functioning as the voltage sensing leads. Current excitation was supplied by an Agilent power supply while the temperature and voltage signals were processed by a calibrated National Instruments DAQ system and analog signal conditioner. The digitized signals were used to calculate a resistance value for each specimen, which in turn allows for the calculation of the samples resistivity, after having appropriately accounted for changes in the sample dimensions due to thermal expansion. The transformation temperatures were also determined by measuring the strain-temperature response of the material under essentially zero load (stress free condition) using the mechanical test setup described below.

2.2 Mechanical Testing

Mechanical testing was performed using an MTS servo-hydraulic test frame equipped with an MTS Flextest SE controller. Hydraulic collet grips with a hot grip insert were used to hold the threaded specimens. A 22 kip load cell was used, and strain measurements in tension were taken with a 12.7 mm gage length extensometer. The extensometer had a maximum range of +20/-10 % strain and was equipped with 85mm long alumina probes with a v-chisel edge. Strain measurements during compression testing were acquired using a laser extensometer. Both tension and compression specimens were induction heated using an Ameritherm Novastar 7.5 power supply. All temperatures were acquired through the use of K-type thermocouples, which were directly spot-welded to the sample. Temperature gradients across the gauge were calibrated to within +/-0.5% of the test temperature.

Monotonic tensile tests were conducted in strain control at a rate of 1×10^{-4} sec^{-1}. Tensile specimens were run to failure or until the 20% strain limit of the extensometer was reached, in which case the samples were unloaded prior to fracture. Compression samples were run in displacement control at a rate which approximately yielded the same initial strain rate as the tension tests. Shape memory behavior was measured using unconstrained or load free strain recovery tests. During this test, specimens were deformed in tension in strain rate control at a rate of 1×10^{-4} sec^{-1} to the required strain level at 100 °C. At this point the controller was switched to load control and the load was reduced to 0 N. Load was held at 0 N while the specimens were thermally cycled to a temperature in the range of 400 ºC. Heating rates were maintained at 10 ºC/min after which the samples were allowed to air cool to 100 °C before repeating the process starting at the next larger strain increment.

The work characteristics of the material were determined from constant load, strain versus temperature tests (referred to as load-bias tests). Specimens were strained at room temperature to the required load in strain control at a rate of 1×10^{-4} sec^{-1}. At this point the controller was switched to load control to maintain the desired load. Specimens were then thermally cycled twice from room temperature to about 100 ºC above the austenite finish temperature. Heating rates were maintained at 10 ºC/min. In tension, the load bias tests were run in a series of increasing loads on the same sample, the specimen was unloaded at room temperature and then strained again to the next higher load level, at which point the thermal cycling process was repeated. The specific work output of the alloy was determined by measuring the resultant change in strain during the martensite-to-austenite transformation during the second heating cycle and multiplying by the stress applied during the thermal cycle. Compression load bias tests were run in a parallel procedure but with the loading phase in displacement rate control rather than strain rate control.

Since it was very difficult to determine a linear elastic region in these samples, even with extensometry, modulus was determined by a dynamic technique using the impulse excitation of vibration method as described in ASTM Standard

E1876 [15]. A rectangular sample, 7.9 mm in width, 3 mm in thickness, and 49 mm long was heated in a furnace at a rate of 3.3 °C/min. Oxidation was minimized by backfilling the furnace with argon. The tests were conducted between 20 and 800 °C taking data every 5 °C during heating only. The samples were impacted with a ceramic projectile creating a flexural mode of vibration and the resulting frequency was measured using a microphone. This frequency was related to Young's modulus by the equations given in reference [15].

3.0 RESULTS AND DISCUSSION

3.1 Material Characterization

A total of six ingots were cast, homogenized, and extruded for use in this and follow on studies. The average composition of the six extrusions was 50.5 ± 0.1 at.% Ti, 19.4 ± 0.2 at.% Ni, 29.4 ± 0.2 at.% Pd, 0.44 ± 0.03 at.% C, and 0.28 ± 0.03 at.% O. Within the resolution of the chemical measurement techniques, none of the individual ingots were discernibly different in composition from each other or the aim composition. In addition, oxygen and carbon (due to the use of graphite crucibles) were present in essentially equal levels within all the extrusions.

The microstructure of the extruded and stress relieved material is shown in Figure 1. The alloy was martensitic at room temperature and predominantly single phase containing a small volume percent of second phase particles. Both x-ray and electron diffraction confirmed that the martensite phase was the B19 (orthorhombic) phase typically observed in ternary alloys with greater than 10 at.% Pd [3,5]. The lattice parameters were a_o = 0.277 nm, b_o = 0.447 nm, and c_o = 0.474 nm. There were two types of second phases present, an intermetallic phase containing Ti, Ni and Pd and the other containing a high amount of Ti tied to the interstitials, C and O. Between electron diffraction and energy dispersive spectroscopic (EDS) analysis, it was determined that the former phase was $Ti_2(Ni,Pd)$, which is isostructural to the face-centered-cubic Ti_2Ni phase commonly observed in Ti-rich NiTi alloys. The $Ti_2(Ni,Pd)$ phase had a lattice parameter a_o = 1.16 nm. Ti_2Ni has a high solubility for interstitially located oxygen [16] and given the high oxygen content in this material the $Ti_2(Ni,Pd)$ probably contained some oxygen as well. The other phase was a typical fcc structured Ti(C,O) with a_o = 0.44 nm. The oxycarbide particles ranged in size from about 0.5 to 2 μm in diameter. The $Ti_2(Ni,Pd)$ phase was blocky in morphology and ranged from 2-6 μm in size. This phase formed interdendritically during melting and then was broken up during the extrusion process. The total volume fraction of second phase particles was less than 5%. It should be noted that no fine precipitate phase was observed in this alloy as reported by Shimizu et al. [6], nor were any phase transformations observed during differential thermal analysis of the alloy up to 1000 °C, other than the martensitic transformation.

The temperature dependence of the resistivity and the strain temperature response of the material determined under zero load conditions are plotted in Figure 2. The transformation temperatures were determined from this data by constructing linear, polynomial curve fits through the low temperature, intermediate temperature, and high temperature portions of the heating and cooling curves, respectively. Through the utilization of the equations for these best fits, start and finish temperatures were determined by interrogating the intersection points. The resulting transformation temperatures determined by the resistivity and strain measurements can be found in Table 1. There was excellent agreement between the two techniques. Given the substantial differences in the electrical properties between the parent B2 and martensite phases, it is apparent why resistance measurement is a prominent characterization technique in the study of shape memory alloys. The technique can be used as an in-situ probe for determining the microstructural changes that occur in a material not only as a function of temperature but also as a function of stress as demonstrated later in this paper. The design of resistance heated SMA actuated devices also requires an understanding of the temperature dependence of the electrical resistance of these alloys in order to determine power requirements for actuators. The thermal expansion behavior of the martensite and austenite phases were similar with the measured coefficients of thermal expansion being 16×10^{-6} and 11×10^{-6} $°C^{-1}$ for the martensite and austenite phase, respectively. The volume change associated with the martensite-to-austenite transformation resulted in an axial strain change along the length of the sample of nearly 0.2%.

Table 1: Transformation Temperatures and Hysteresis for $Ni_{19.5}Pd_{30}Ti_{50.5}$

Transformation Temperature (°C)	Measurement Technique	
	Dilatometry	Resistance
A_s	250	256
A_f	257	260
M_s	249	249
M_f	238	239
Hysteresis (A_f - M_s)	8	11

3.2 Isothermal Stress-Strain Behavior in Tension and Compression

Representative true stress - true strain curves for the $Ni_{19.5}Pd_{30}Ti_{50.5}$ alloy in tension and compression are shown in Figures 3 and 4. All isothermal stress strain curves are shown in true stress - true strain, thus allowing for the direct comparison of the mechanical properties in tension and compression. Figure 3 is a plot of the stress strain relationship of the austenite and martensite phases well above or below the transformation temperatures, while Figure 4 shows the isothermal mechanical behavior of the $Ni_{19.5}Pd_{30}Ti_{50.5}$ alloy between or very near the transformation temperatures.

Isothermal tension and compression tests revealed that the yield stresses in both modes were comparable over the range of temperatures investigated and that the general characteristics of the stress-strain curves were similar except for samples tested below the martensite finish temperature (M_f) (Figure 3). The room temperature (RT) and 200 °C tensile curves (Figure 3a) exhibited a "pseudo-stress" plateau or region of low hardening rate at stress levels starting about 250 MPa. While this pseudo-stress plateau was not nearly as dramatic as that observed in binary NiTi alloys [17], it was still attributed to the reorientation of favored martensite variants, since deformation in this regime was thermally recoverable (as described in section 3.4). In contrast, no discernable stress plateau was observed in compression and a high work hardening rate was observed from the onset of yielding out to strains of about 10% indicating a much greater resistance to deformation. Deformation by detwinning mechanisms is polar in nature, in contrast to slip behavior, such that a reversal in the shear direction will not produce twin movement in variants favorably aligned for operation in the forward direction [18]. In other words, twins aligned favorably for operation in compression will not operate under a tensile stress and vice versa. Apparently the manner in which the material was processed (extrusion in this case) resulted in a more favorable variant structure for detwinning in tension than compression. Additional testing and microstructural characterization of deformed samples are planned to elucidate the actual deformation mechanisms operating in the martensite phase in compression and after the stress plateau in tension.

Well above the transformation temperature, the mechanical properties of the austenite were comparable in tension and compression (Figure 3a & b). After yielding, the material exhibited a low work hardening rate that decreased with increasing isothermal test temperature. In the 400 °C tensile and 500 °C compression tests the $Ni_{19.5}Pd_{30}Ti_{50.5}$ alloy exhibited a slight work softening due to recovery processes that become dominate at elevated temperatures.

For the results shown in Figure 4a and 4b, the samples were heated to well above the austenite finish temperature (A_f) and allowed to cool back to the test temperature before applying load to the samples. The process of heating significantly beyond the A_f and subsequently cooling back to test temperatures of 255 and 272 °C ensured that the resulting stable phase was that of austenite, since the martensite start temperature (M_s) was 249 °C. In-situ resistivity measurements and the occurrence of a well defined stress plateau indicated that upon loading in either tension or compression, stress induced martensite is formed. This behavior can be seen in detail in Figure 5, which is a superimposed plot of resistivity, determined in-situ during compression testing at 255 °C, with the stress - strain data. The resistivity initially increased with strain during elastic deformation of the austenite, and then immediately decreased as stress induced martensite was formed (the resistivity of austenite is larger than that of the martensite as shown Figure 2, hence the decrease in resistivity). For both tension and compression, the relative amounts of stress induced martensite as well as the stress at which the transformation occurred were comparable. For tensile samples deformed below the M_s (225 and 245 °C), deformation was similar to that of martensite at other temperatures, shown previously in Figure 3a. Finally, a tensile ductility minimum was observed in the region where the stress induced martensite occurred, similar to the behavior reported in NiTiPt shape memory alloys [19].

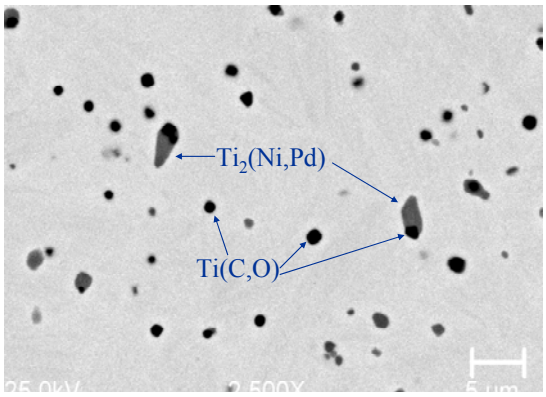

Figure 1. Backscattered electron image of the microstructure of the extruded $Ni_{19.5}Pd_{30}Ti_{50.5}$ alloy. At room temperature, the alloy is an orthorhombic structured martensite, which contains a small volume fraction of TiC (fine black particles) and $Ti_2(Pd,Ni)$ (larger gray phase).

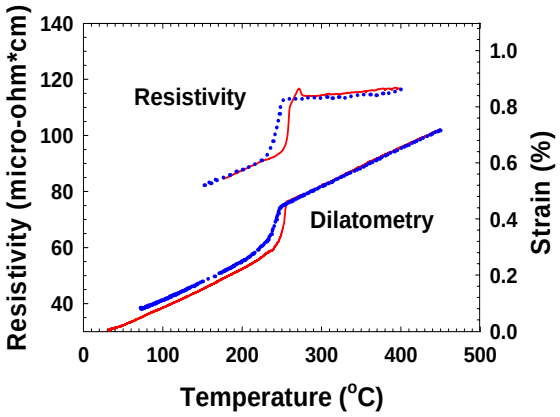

Figure 2. Electrical resistivity and strain versus temperature for $Ni_{19.5}Pd_{30}Ti_{50.5}$. Corresponding transformation temperatures determined by these two techniques are listed in Table 1.

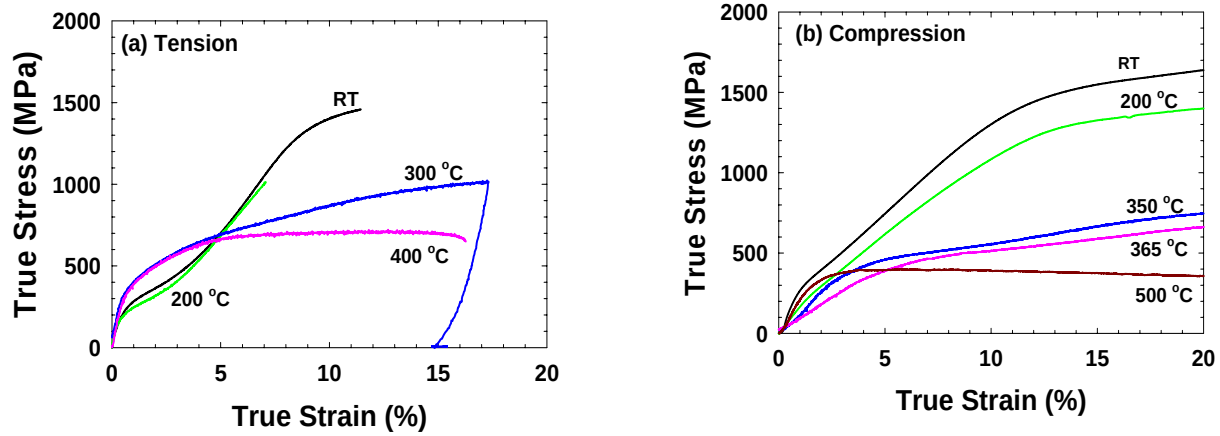

Figure 3. Representative true stress - true strain behavior for $Ni_{19.5}Pd_{30}Ti_{50.5}$ at temperatures significantly above or below the transformation temperature of the alloy determined in a.) tension and b.) compression.

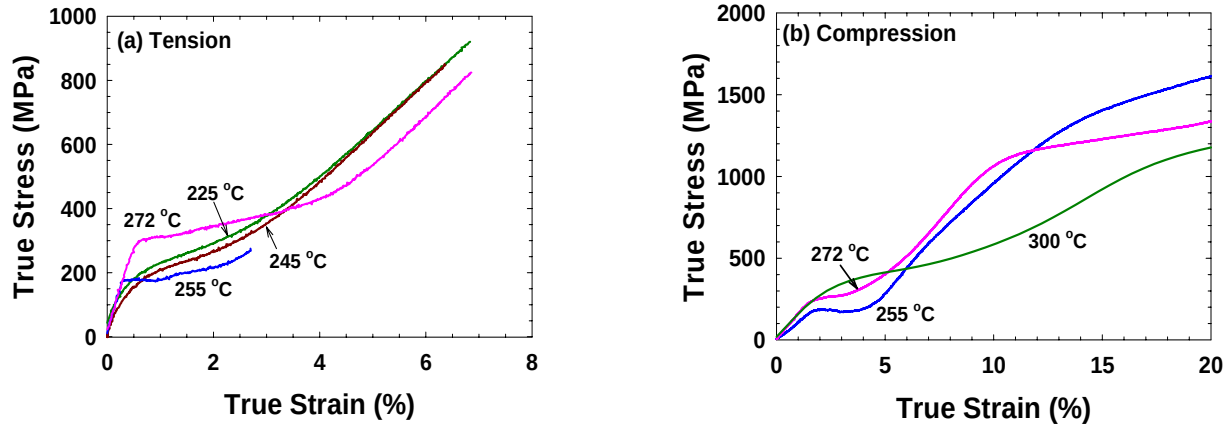

Figure 4. Representative true stress - true strain behavior for $Ni_{19.5}Pd_{30}Ti_{50.5}$ at temperatures within or near the transformation hysteresis in a.) tension and b.) compression.

The temperature dependence of the yield stress in compression and tension, determined from the proportional limit of the isothermal stress strain curves, is shown in Figure 6. Generally, the yield stress in tension and compression were similar at a given temperature. The yield stress of the martensite decreased with increasing temperature and reached a minimum near the A_f. Beyond this minimum the alloy was austenitic (though the formation of stress-induced martensite was possible) and the yield strength increased significantly with increasing test temperature until a peak near 350 °C. At temperatures above 400 °C the austenite weakened and the onset of slip occurred at lower stresses. It is important to note that the yield stress for the martensite represents the stress at which detwinning begins, while yielding of the austenite phase is due to plastic deformation by dislocation processes.

3.3 Dynamic Modulus

It was very difficult to define a linear elastic region from the tensile and compression tests, especially at temperatures near or below the transformation temperature of the alloy as the elastic modulus was very dependent on strain level. Therefore, in order to have an accurate representation of the elastic modulus of these materials as a function of temperature a dynamic modulus test was conducted. The modulus - temperature relationship is plotted in Figure 7, and has three main regions corresponding to the material in the fully martensitic condition, the two-phase martensite plus austenite region that exists between A_s and A_f, and the fully austenitic phase. The dynamic modulus of the martensite at room temperature was just over 20 GPa higher than that of the austenite at A_f, but decreased with temperature. In contrast, the modulus increased slightly with temperature for the fully austenitic material suggesting that the stability of this phase was increasing with increasing temperature up to about 750 °C. The region bound by the transformation A_s and A_f temperatures exhibited a stronger temperature dependence than did either of the single phases. The modulus within this regime was proportional to the effective modulus of the resulting transformation products in the two-phase martensite plus austenite region, terminating at a minimum of 59 GPa at the A_f. At this point the material was fully austenitic and the modulus value was that of the austenite at the transformation temperature. It should be noted that the temperatures in Figure 7 were corrected to account for the fact that the actual sample temperature was not measured during the test. Because the martensite-to-austenite transformation is very endothermic, it suppresses the actual temperature of the sample compared to the furnace temperature. The thermocouple used to record the sample temperature for the modulus measurements was near but not touching the sample, since a directly attached thermocouple would interfere with the modulus measurements. In contrast, thermocouples were spotted welded directly to the resistivity and dilatometry samples used to generate the data in Figure 2.

3.4 Shape Memory Behavior

Shape memory behavior is the ability of a material to recover twinning-induced deformation that is introduced at temperatures below the martensite finish temperature by heating the material through its transformation temperature. In practice [6-13], it is simply determined by measuring the amount of strain introduced into a sample during deformation below the M_f, heating the sample through the transformation above the A_f, and cooling back usually to room temperature where the final dimensions of the sample are measured and used to determine the amount of strain recovered. However, if one were to monitor the strain - temperature response of the material continuously during this process, as shown in Figure 8a, it is apparent that a number of different mechanisms contribute to the overall strain recovery of NiTiPd alloys as first reported by Lindquist [20]. Figure 8a shows the strain temperature response of the $Ni_{19.5}Pd_{30}Ti_{50.5}$ alloy as it was loaded to approximately 2% total strain and unloaded at 100 °C, resulting in approximately 1% "plastic" deformation. This was followed by heating to 400 °C and cooling back to 100 °C in an unconstrained condition. Three contributing factors to strain recovery can be identified in Figure 8a: (1) Continuous shape recovery began on heating up to the A_s temperature and the amount of recovery was estimated from the differences between the deformed martensite strain – temperature heating curve and the original undeformed martensite thermal expansion behavior taken from Figure 2. This difference may be the result of the rearrangement of twins in the material due to the initial deformation, such that the expansion characteristics of the detwinned material along this one direction may no longer be the same as measured in a sample with a more randomly oriented martensite. However, no attempt was made to confirm this through microscopic observations of the sample structure. (2) The majority of the strain recovery occurred between A_s and A_f but there were really two competing effects. There was a volume increase due to the transformation from martensite to the austenite phase and there is the typical strain recovery due to the shape memory effect, which was generally the overriding factor for strain change in samples deformed to greater than 1% plastic strain. (3) Finally, there was the strain change attributed to the volume decrease as the material transformed back from austenite to martensite. However, this strain does not necessarily have to be equivalent to the strain change on heating of the deformed sample for essentially

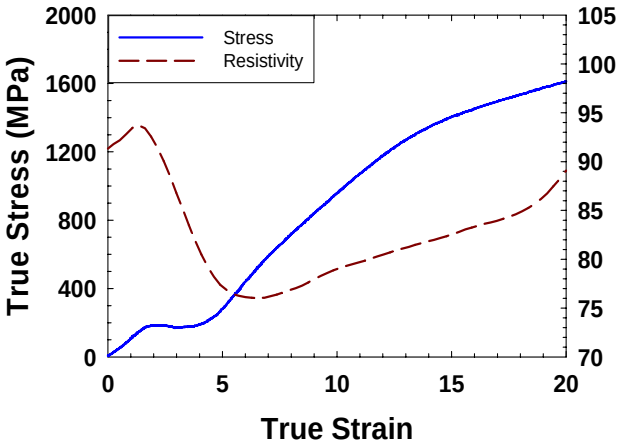

Figure 5. Stress - strain behavior and corresponding in-situ resistivity - strain measurements for $Ni_{19.5}Pd_{30}Ti_{50.5}$ tested at 255 °C. The stress plateau and resistivity behavior are indicative of stress induced martensite at this temperature.

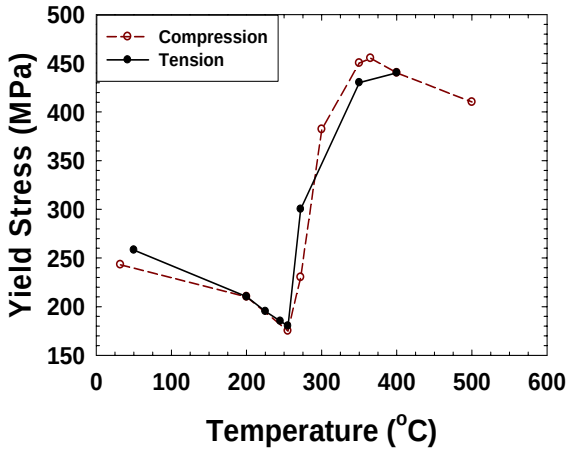

Figure 6. Yield strength (proportional limit) determined in tension and compression as a function of temperature for $Ni_{19.5}Pd_{30}Ti_{50.5}$.

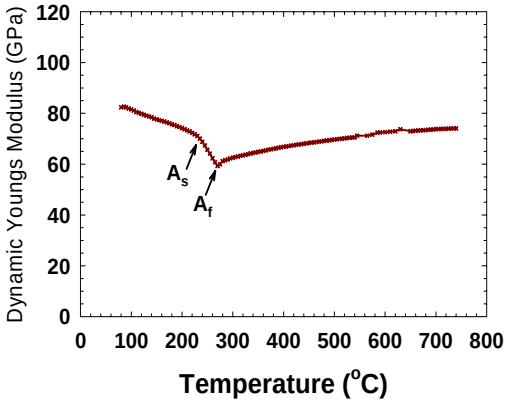

Figure 7. Dynamic modulus for $Ni_{19.5}Pd_{30}Ti_{50.5}$ as a function of temperature determined on heating between room temperature and 750 °C.

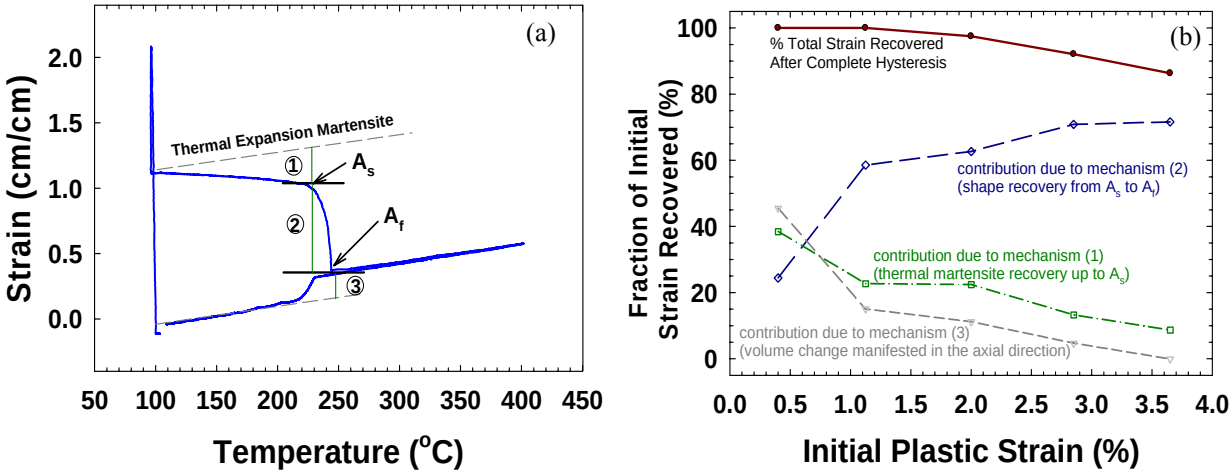

Figure 8. a.) Unconstrained strain - temperature response of $Ni_{19.5}Pd_{30}Ti_{50.5}$ deformed to 2% strain at 100 °C unloaded and heated through the transformation temperature and cooled back to 100 °C. The various mechanisms that contribute to the total strain recovery of the material are defined on the plot. b.) Percent plastic strain recovered after thermal cycling versus initial plastic strain introduced in the sample and each of the components that make up the total strain recovered.

the same reasons as discussed for thermal expansion differences that occur in region 1. Furthermore, as the initial strain introduced in the sample increased, the strain measured along the deformation axis, due to the volume decrease on cooling from austenite to martensite, was found to decrease significantly, as shown in Figure 8b. This may be attributed to nucleation of a preferred orientation of martensite on cooling due to the dislocation structure generated in the material during plastic deformation of the martensite at the larger initial strains, but was not confirmed experimentally.

The overall strain recovery as a percent of the initial plastic strain introduced into the sample at 100 °C is plotted as a function of initial plastic strain in Figure 8b. The $Ni_{19.5}Pd_{30}Ti_{50.5}$ alloy is capable of recovering 100% of the initial plastic strain introduced into the sample up to an initial plastic strain of 1% and is capable of recovering over 80% of the initial plastic strain at levels up to 3.5%. Different research groups plot this type of recovery information in slightly different forms but our results are consistent with those previously published for NiTi-30Pd alloys [5-7, 10-12]. The individual contributions of the total strain recovery are also shown in Figure 8b as a function of initial plastic strain and are labeled (1)-(3), respectively, corresponding to the discussion of these mechanisms in the previous paragraph and as defined in Figure 8a.

3.5 Constant-Load, Strain-Temperature Tests and Work Output

Given the significant amount of research performed on unconstrained shape recovery of NiTi-30Pd alloys [5-13], it is surprising that no investigation of constrained recovery has been reported. This is especially astounding given the fact that the primary application for high-temperature shape memory alloys (HTSMA) such as NiTiPd would be for use as solid state actuator materials where work output (or the ability of the material to recover strain against some biasing force) is the primary consideration. Consequently, load bias testing was performed on the $Ni_{19.5}Pd_{30}Ti_{50.5}$ alloy in order to quantify the work output of the material as a function of the applied stress and mode of application (uniaxial tension or compression).

For the constant-load, strain-temperature testing, the load was applied to the sample at room temperature and then held constant as the sample was heated and cooled through the transformation. During this process, the strain in the sample due to the initial applied load at room temperature, prior to any thermal cycling, was always much smaller than when the sample was cooled through the transformation while under load. As a result, the transformation strain during the initial heating cycle was also much smaller than in successive cycles. This behavior is clearly demonstrated in Figure 9, which shows the initial loading and then two complete heating and cooling cycles for the $Ni_{19.5}Pd_{30}Ti_{50.5}$ alloy under a tensile stress of 99 MPa. This type of behavior is quite common in conventional NiTi alloys [21] and is also observed in NiTiPt shape memory alloys [19]. There are probably several contributing factors: 1) The yield strength of the martensite phase decreases with increasing temperature reaching a minimum at the transformation temperature for the alloy. This effect would be expected to contribute to the increased strain by the unfavorable mechanism of plastic deformation. Evidence for the operation of this mechanism can be seen in the fact that the strain - temperature hysteresis loops do not close, with the strain on cooling through the transformation regime always being larger than the strain on heating. This results in permanent deformation of the alloy. 2) The dynamic Young's modulus for the martensite phase decreases significantly with increasing temperature from approximately 82 GPa at room temperature to a minimum of about 58 GPa at the A_f temperature. 3) The largest contribution to the enhanced strain is probably due to the nucleation of preferred variant orientations of martensite during cooling under load, which favor the applied strain. In other words, cooling under load begins to "train" the material, resulting in a greater fraction of favorably oriented martensite variants that can accommodate a larger strain in the sample for a given stress.

Because of the difference in the level of strain developed in the material during loading at room temperature versus cooling through the transformation temperature under load, the first complete heating and cooling cycle at each stress level in the load-bias tests were ignored and only the second complete cycle or hysteresis is plotted in Figures 10a & b. Figure 10 shows the results of the strain – temperature behavior of the HTSMA at various stress levels for both tensile and compression loading. It is interesting to note that the strain - temperature response of the $Ni_{19.5}Pd_{30}Ti_{50.5}$ under load (Figure 10) was actually much simpler than that observed under stress free conditions (Figure 8a), with essentially all the strain change (due to shape recovery and plastic deformation) occurring within transformation region of the alloy. In addition, the actual transformation temperatures were found to increase with applied stress. At 393 MPa, the transformation temperatures were $A_s = 285$, $A_f = 317$, $M_s = 299$, and $M_f = 267$ °C, or an average increase of about 42 °C.

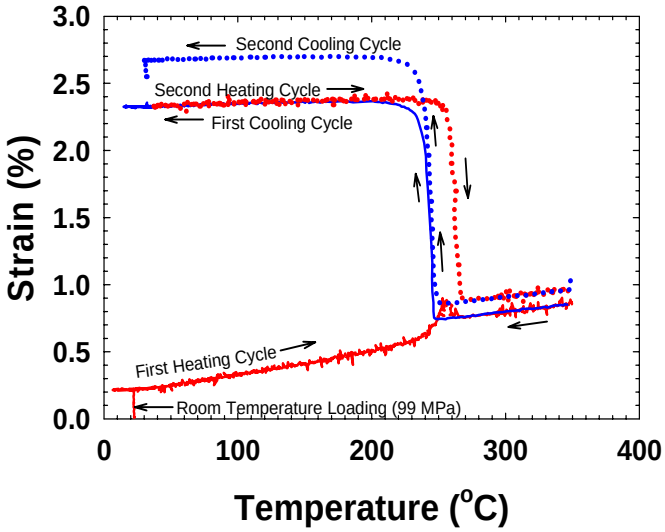

Figure 9. Initial loading and first two complete constant stress (99 MPa), strain-temperature cycles for $Ni_{19.5}Pd_{30}Ti_{50.5}$. First complete heating and cooling cycle is represented by solid lines and the second complete heating and cooling cycle by dotted lines.

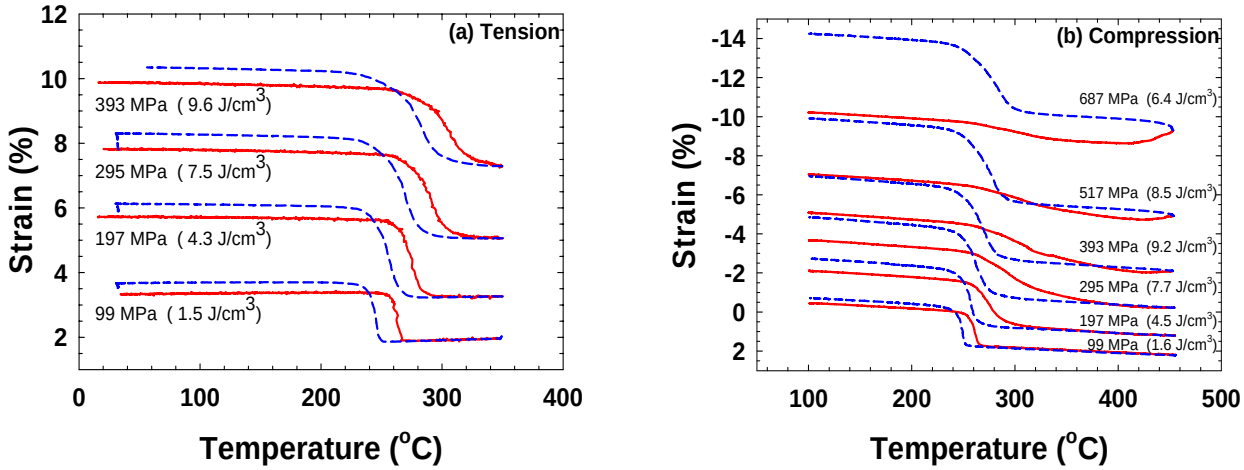

Figure 10. Load biased, strain – temperature response of the $Ni_{19.5}Pd_{30}Ti_{50.5}$ alloy at different stress levels in a.) compression and b.) tension. Solid lines are heating curves and dashed lines represent the material response on cooling. The constant stress level and resulting work output are indicated for each set of curves.

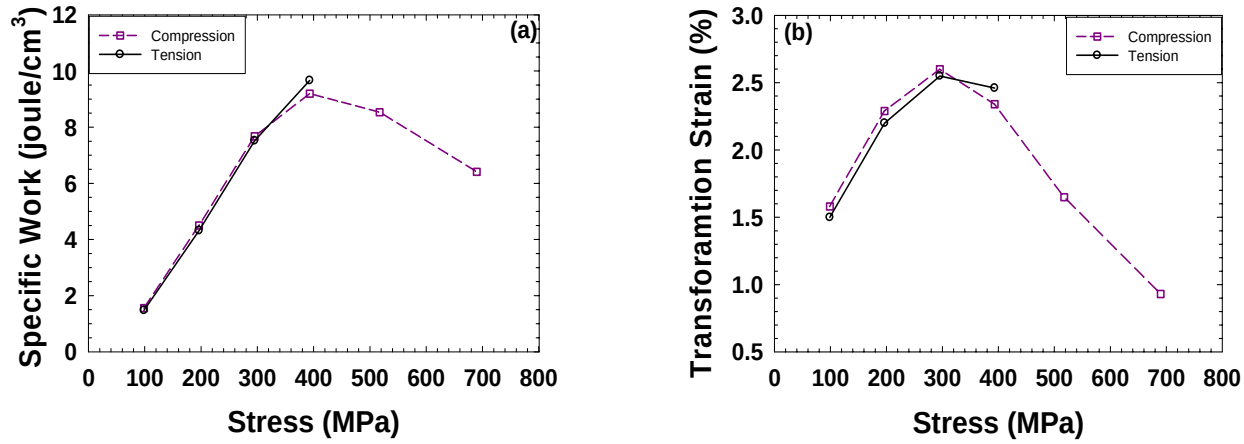

Figure 11. a.) Specific work output for $Ni_{19.5}Pd_{30}Ti_{50.5}$ as a function of applied stress loaded in both tension and compression and b.) The corresponding transformation strain versus applied stress.

The specific work output was calculated by simply multiplying the transformation strain on heating by the applied constant stress for each set of load bias curves in Figure 10. In order to more easily compare the behavior of the $Ni_{19.5}Pd_{30}Ti_{50.5}$ alloy in tension and compression, the specific work output was plotted versus stress level (Figure 11a). In this case, the work output in tension and compression as a function of stress was essentially identical. There were no significant anisotropic (tension versus compression) effects observed in the load-bias testing. The reason for the lack of anisotropy was due to the way the tests were run. By running two complete thermal cycles on the material at each load level such that the material was actually cooled through the transformation temperature under load, it was possible to nucleate martensite variants with a favorable orientation along the principal stress axis, maximizing the transformation strain on heating. As such, tests conducted in tension contained a variant structure that was optimized for tensile loading while tests conducted in compression contained a structure optimized for compressive loading. Overall, the specific work output increased with increasing stress level until a maximum work output of about 9 J/cm^3 was attained at approximately 400 MPa and then began to decrease with further increases in stress. This peak is evident from the compression data as the tensile data reaches a maximum at the peak and was limited by failure of the sample during testing at the higher stress levels due to limitations in tensile ductility, which, as shown in Figure 4a, reaches a minimum within the region where the transformation occurs.

In general the work output - stress behavior of the $Ni_{19.5}Pd_{30}Ti_{50.5}$ was similar to that observed in conventional NiTi alloys. Conventional NiTi alloys exhibit a peak in the work output with maximum values of 10 - 20 J/cm^3 [19,21,22]. This peak in work output is due to competing factors. As the stress level increases, eventually the stresses become large enough that they begin to prevent complete recovery of the material during heating, causing the transformation strain to eventually reach a maximum and then rapidly decrease with increasing stress as shown in Figure 11b for the $Ni_{19.5}Pd_{30}Ti_{50.5}$ alloy. Therefore, even though the applied stress is increasing, the transformation strain begins to decrease and the product of the applied stress and transformation strain, which is work output, reaches a maximum at a particular stress level.

However, having a work output that falls within the lower range of conventional NiTi alloys is still not sufficient for use of the $Ni_{19.5}Pd_{30}Ti_{50.5}$ alloy in actuator applications where repeated cycling is necessary. At every stress level investigated, the strain-temperature curves did not close at the end of the test (Figure 10). The amount of plastic deformation or open loop strain, determined by the strain difference between the heating and cooling curves at low temperature, is plotted as a function of stress in Figure 12. In tension, this permanent deformation was attributed to the larger strain that developed on cooling through the transformation than on heating due to non-recoverable deformation of the martensite phase. The amount of permanent deformation that resulted increased with increasing stress. The alloy suffered from plastic or permanent deformation even at stresses as low as 99 MPa, even though for isothermal monotonic testing of this alloy, gross yielding was not observed until stresses in the neighborhood of 170 MPa near the transformation temperature. At stresses above 200 MPa the amount of permanent deformation observed during compression loading deviated considerably from the tensile samples. This was due to the manner in which the tests were conducted with the tensile tests cycled under load only to 350 °C while the compression tests were cycled to 450 °C. Due to the higher temperature, the austenite phase during compression testing also underwent significant plastic deformation, which increased with increasing stress.

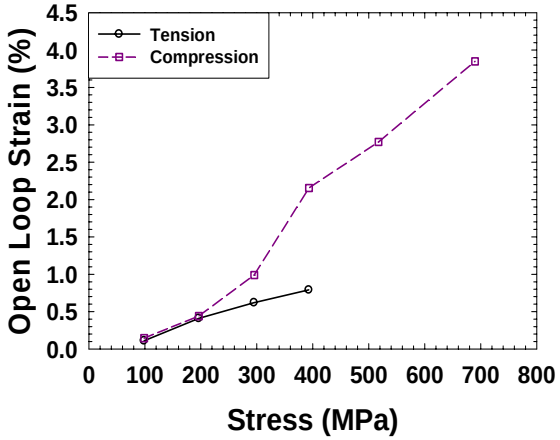

Figure 12. The amount of plastic deformation (open loop strain) associated with each stress level of the load-bias tests performed in tension and compression. It should be noted that the excessive plastic deformation in compression, compared to the tensile behavior, was due to plastic deformation of the austenite, since the compression tests were run to higher temperatures.

This type of dimensional instability is unacceptable since continued cycling of the temperature while under load would cause the material to ratchet or "walk" with each cycle, very quickly exhausting the fatigue life of the sample and eventually resulting in failure. Even if fracture was postponed for a significant number of cycles, changes in length during use of an actuator would cause drifting of the zero point and possible loss of control. The problem is in part the same as that originally observed for the poor stress-free shape memory performance of TiPd and NiTiPd alloys [6,10,11], namely that deformation by recoverable twin mechanisms occurs at almost the same stress levels for which non-recoverable mechanisms begin to operate. Therefore, it is necessary to find a method to increase the resistance of the martensite phase to deformation by non-recoverable processes. Over temperature conditions, while under load, are also a serious consideration with this material and therefore increasing the strength of the austenite phase would also be advisable. The obvious mechanisms for increasing the strength of both phases are the same as those proposed by Otsuka et al. [10] for trying to improve the unconstrained shape memory behavior of TiPd, which include 1.) solute strengthening, 2.) precipitate strengthening, or 3.) thermomechanical processing. Consequently, while NiTiPd alloys, especially with higher Pd contents for use between 200 and 300 °C, posses attributes that make them promising for high-temperature shape memory applications (such as high transformation temperatures, narrow hysteresis, good work output, and reasonable mechanical properties), there is still quite a bit of development that needs to be done before a viable HTSMA is produced from this system.

4.0 SUMMARY AND CONCLUSIONS

We have characterized the mechanical behavior of a $Ni_{19.5}Pd_{30}Ti_{50.5}$ high-temperature shape memory alloy in both uniaxial tension and compression at various temperatures and loading schemes. Differences in the isothermal deformation behavior of the alloy were only notable at test temperatures below the martensite finish temperature, with a slight tension - compression anisotropy in the flow behavior observed. Overall, the alloy exhibited a minimum in dynamic modulus, yield strength, and tensile ductility at the transformation temperature of the alloy.

The strain-temperature response of the $Ni_{19.5}Pd_{30}Ti_{50.5}$ alloy under various loads was also determined in both tension and compression and the specific work output determined. There were essentially no effects of loading direction on the work properties of the alloy. As with conventional NiTi alloys the work output increased with stress level, reached a maximum and then decreased with further increase in stress. This was due to the behavior of the transformation strain which exhibited a similar trend with stress. Unfortunately, the alloy exhibited non-recoverable plastic deformation at nearly every stress level investigated. Consequently, before this alloy can be used under cyclic actuation conditions, modification of the microstructure or composition would be required to increase the resistance of the martensite and austenite phase to plastic deformation by slip.

ACKNOWLEDGEMENTS

The authors wish to thank Jami Olminski for performing the compositional analyses. Useful discussions and the patience of A. Tenteris and N. Noebe are greatly appreciated. O. Rios wishes to acknowledge financial support from the NASA GSRP and the guidance of Profs. Michael Kaufman and Hans Seifert. This work was sponsored by the IR&D fund at the NASA Glenn Research Center with additional support from the Fundamental Aeronautics – Supersonics project office.

REFERENCES

1. K. Otsuka and X. Ren, "Physical metallurgy of Ti-Ni-based shape memory alloys," *Prog. Maters. Sci.* **50**, 511-678, 2005.
2. H.C. Donkersloot and J.H.N. Van Vucht, "Martensitic Transformations in Gold-Titanium, Palladium-Titanium and Platinum-Titanium Alloys Near The Equiatomic Composition," *J. Less Com. Met.* **20,** 83-91**,** 1970.
3. N.G. Boriskina and E.M. Kenina, "Phase Equilibria in the Ti-TiPd-TiNi System Alloys," in *Titanium 80, Science & Technology, Proceedings of the 4th International Conference on Titanium*, H. Kimura and O. Izumi, eds., pp. 2917-2927, The Metallurgical Society of AIME, Warrendale, PA., 1980.

4. V.N. Khachin, "Martensitic transformation and shape memory effect in B2 intermetallic compounds of titanium," *Revue Phys. Appl.* **24**, 733-739, 1989.
5. P.G. Lindquist and C.M. Wayman, "Shape Memory and Transformation Behavior of Martensitic Ti-Pd-Ni and Ti-Pt-Ni Alloys," in *Engineering Aspects of Shape-memory Alloys*, T.W. Duerig, K.N. Melton, D. Stockel and C.M. Wayman, eds., pp. 58-68, Butterworth-Heinemann, London, 1990.
6. S. Shimizu, Y. Xu, E. Okunishi, S. Tanaka, K. Otsuka and K. Mitose, "Improvement of shape memory characteristics by precipitation-hardening of Ti-Pd-Ni alloys," *Maters. Lett.* **34**, 23-29, 1998.
7. Q. Tian and J. Wu, "Characterization of mechanical properties of $Ti_{50.6}Ni_{19.4}Pd_{30}$ alloys showing different phase transformation behaviors," in *Smart Sensors, Actuators, and MEMS*, pp. 710-717, SPIE Conf. Proc. Vol. **5116**, 2003.
8. W.S. Yang and D.E. Mikkola, "Ductilization of Ti-Ni-Pd Shape Memory Alloys With Boron Additions," *Scripta Metall. Mater.* **28,** 161-165, 1993.
9. V.N. Kachin, N.M. Matveeva, V.P. Sivokha, D.B. Chernov and Yu. K. Koveristyi, "High-Temperature Shape-Memory Effects in Alloys of the TiNi-TiPd System," *Doklady Akad. Nauk SSSR* **257**, 195-197, 1981.
10. K. Otsuka, K. Oda, Y. Ueno, M. Piao, T. Ueki, H. Horikawa, "The Shape Memory Effect in a $Ti_{50}Pd_{50}$ Alloy," *Scripta Metall. Mater.* **29** 1355-1358, 1993.
11. Y. Suzuki, Y. Xu, S. Morito, K. Otsuka, K. Mitose, "Effects of boron addition on microstructural and mechanical properties of Ti-Pd-Ni high temperature shape memory alloys," *Maters. Lett.* **36**, 85-94, 1998.
12. D. Goldberg, Y. Xu, Y. Murakami, S. Morito, K. Otsuka, T. Ueki, and H. Horikawa, "Improvement of $Ti_{50}Pd_{30}Ni_{20}$ High Temperature Shape Memory Alloy by Thermomechanical Treatments," *Scripta Metall. Mater.* **30**, 1349-1354, 1994.
13. W. Cai, S. Tanaka, and K. Otsuka, "Thermal Characteristics Under Load in a $Ti_{50.6}Pd_{30}Ni_{19.4}$ Alloy," *Maters. Sci. Forum* **327-328**, 279-282, 2000.
14. D.S. Grummon, "Thin-Film Shape-Memory Materials for High-Temperature Applications," *JOM* **55 (12)**, 24-32, 2003.
15. "Standard Test Method for Dynamic Young's Modulus, Shear Modulus, and Poisson's Ratio by Impulse Excitation of Vibration," ASTM E1876-01, Annual Book of ASTM Standards, Vol. 03.01, pp. 1122-1137, ASTM International, West Conshohocken, PA, 2004.
16. M.V. Nevitt, "Stabilization of Certain Ti_2Ni-Type Phases by Oxygen," *Trans. Metall. Soc. AIME* **218**, 327-331, 1960.
17. C.M. Wayman and T.W. Duerig, "An Introduction to Martensite and Shape Memory," in *Engineering Aspects of Shape Memory Alloys*, T.W. Duerig, K.N. Melton, D. Stockel, and C.M. Wayman, eds., pp. 3-20, Butterworth-Heinemann, Boston, 1990.
18 K. Gall, H. Sehitoglu, Y. I. Chumlyakov and I. V. Kireeva, "Tension and compression asymmetry of the stress strain response in aged single crystal and polycrystalline NiTi," *Acta mater*. **47**, 1203-1217, 1999.
19. R. Noebe, D. Gaydosh, S. Padula, A. Garg, T. Biles, and M. Nathal, "Properties and Potential of Two (Ni,Pt)Ti Alloys for Use as High-Temperature Actuator Materials," in *Smart Structures and Materials 2005: Active Materials: Behavior and Mechanics*, pp. 364-375, SPIE Conf. Proc. Vol. **5761**, 2005.
20. P.G. Lindquist, "*Structure and Transformation Behavior of Martensitic Ti-(Ni,Pd) and Ti-(Ni,Pt) Alloys,*" Ph.D. Dissertation, University of Illinois, 1988.
21. T.W, Duerig, D. Stockel, and A. Keeley, "Actuator and Work Production Devices", in *Engineering Aspects of Shape Memory Alloys*, T.W. Duerig, K.N. Melton, D. Stockel, and C.M. Wayman, eds., pp. 181-194, Butterworth-Heinemann, Boston, 1990.
22. W.B. Cross, A.H. Kariotis, and F.J. Stimler, "*NITINOL Characterization Study*," NASA CR-1433, 1969.